ELSEVIER

Colloids and Surfaces
A: Physicochemical and Engineering Aspects 160 (1999) 217–227

COLLOIDS AND SURFACES A

www.elsevier.nl/locate/colsurfa

Dissolution of the barite (001) surface by the chelating agent DTPA as studied with non-contact atomic force microscopy

Kang-Shi Wang [a], Roland Resch [b], Kai Dunn [a], Patrick Shuler [c], Yongchun Tang [c], Bruce E. Koel [b], Teh Fu Yen [a,*]

[a] *Department of Civil and Environmental Engineering, University of Southern California, Los Angeles, CA 90089, USA*
[b] *Department of Chemistry, University of Southern California, Los Angeles, CA 90089, USA*
[c] *Chevron Petroleum Technology Company, La Habra, CA 90631, USA*

Received 29 September 1998; received in revised form 9 March 1999; accepted 22 March 1999

Abstract

DTPA (diethylenetriaminepentaacetic acid) is a chelating agent widely used for removal of barium sulfate (barite) scale in the petroleum industry. In this paper we report ex-situ investigations of barite dissolution in deionized water and in 0.18 M DTPA aqueous solutions. Non-contact atomic force microscopy (NC-AFM) was used to observe dissolution on the $BaSO_4$ (001) cleavage surface. Dissolution was carried out at room temperature in a 10 ml reactor. Each sample was first etched in solution and dried before examination by NC-AFM. Dissolution on the $BaSO_4$ (001) surface took place via development of etch pits. In deionized water, triangular etch pits were observed on the (001) terraces at room temperature. And, zigzag shaped etch pits were found at the edges of steps. In DTPA solutions, etch pits on the (001) terraces were observed and these became deeper and longer with increasing time. The geometry of these etch pits was trapezoidal, and/or trapezohedral. To explain this characteristic morphology caused by dissolution we suggest that the active sites of one DTPA molecule bind to two or three Ba^{2+} cations exposed on the (001) surface.

Keywords: Diethylenetriaiminepentaacetic acid; Chelating agent; Barite; Non-contact atomic force microscopy; Etch pits

1. Introduction

Industrial water, oil and gas production systems suffer considerably from expensive problems caused by mineral scale deposits. In particular, as the petroleum industry injects sea water to raise and maintain pressure of offshore oil-bearing reservoirs for enhanced oil recovery, the formation of adherent scales will contribute to significant problems [1,2]. When the injected sea water containing sulfate (SO_4^{2-}) and carbonate (CO_3^{2-}) anions mixes with the formation water in reser-

* Corresponding author. Tel.: +1-213-740-0586; fax: +1-213-744-1426.
E-mail address: tfyen@mizar.usc.edu (T. Fu Yen)

0927-7757/00/$ - see front matter
PII: S0927-7757(99)00183-1

voirs containing alkaline earth cations (Ca^{2+}, Sr^{2+} and Ba^{2+}), scales in the region of the wellbore are developed for calcium carbonate (calcite), calcium sulfate (anhydrite), strontium sulfate (celestite) and barium sulfate (barite). $BaSO_4$ scale, however, is the most difficult to remove because of its extremely low solubility ($K_{sp} = 10^{-9.99}$ at 25°C) in water [3]. If the scaling water also contains dissolved Ra^{226} or Ra^{228}, then Ra will co-precipitate into the barite and thereby make it radioactive [4]. The disposal of scales containing naturally occurring radioactive materials (NORM) is a serious problem because of stringent environmental regulations. Scales are responsible for many equipment failures, production losses, and radioactive exposures. Tens of millions of dollars are spent every year to prevent the formation of mineral scales or to remove them once they have occurred in the field.

The aim of this paper is to investigate the fundamental chemical interactions underlying one of the techniques currently employed to control scale problems in oil fields, i.e., a chemical method using scale dissolvers (chelating agents). This technology uses chelating agents, which form remarkably stable chelates with alkaline earth cations, and has great potential for practical scale dissolution. Chelating agents with low toxicity and a limited impact on the environment are required. These molecules are typically polyaminocarboxylic acids such as DTPA. DTPA is believed to be the most effective scale dissolver in the petroleum industry since the early studies by Morris and Paul [5] and Putnis et al. [6]. DTPA, an octodentate ligand, forms a strong 1:1 (ligand: metal) chelate in solutions at high pH [7],

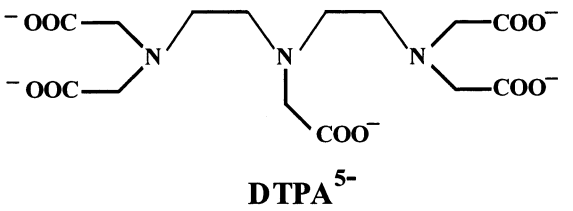

Scheme 1.

binding to the metal center with five carboxylate oxygen atoms and three nitrogen atoms. However, $DTPA^{5-}$ (Scheme 1) exists as a major component in DTPA aqueous solution only at pH values greater than 12. The stability constant $\log K_{ML}$ for $BaDTPA^{3-}$ is 8.78 [8]. But, this constant measures the ability of the ligand to complex metal ions that are free in solution, not from a strongly bound site on an ionic solid like a mineral. The solution-mineral interface equilibrium data and the interfacial reactions that occur there are not well understood. Our approach to improve knowledge about such reactions is based on using Scanning Force Microscopy (SFM) to enable us to observe morphological changes that occur during mineral dissolution. Analysis of these images provides considerable insight to the reaction mechanisms at the molecular level, i.e., the interaction between the DTPA dissolver and the barite surface.

SFM has recently been used to study water-mineral interface reaction processes such as mineral growth and/or dissolution [9–14], mineral growth inhibition [15–17], and mineral etching in solution [18]. Elucidation of these processes is of wide interest in mineral surface science, aqueous geochemistry and environmental chemistry. A widely used imaging procedure is to scan a sample with the tip in permanent contact called contact-mode atomic force microscopy (CM-AFM) with the surface [19]. Deflection of the cantilever induced by small forces acting on the tip reveals the sample's topography. The major drawback of operating a SFM in this mode is the presence of lateral shear forces that can lead to damage or modification of the sample during the scanning process. A related technique that avoids contact between the tip and sample is non-contact mode AFM (NC-AFM) [20,21]. Here, the cantilever oscillates at (or near) its resonant frequency with a tip at a few nanometers above the sample surface. Changes in the oscillation amplitude reveal the topography of the sample. Since the tip is not in contact with the sample surface, damage of the surface and/or surface modification caused by lateral shear forces [22] or intermittent contact [23] can be excluded.

2. Experimental methods

2.1. Barite crystal

Natural barite crystals were obtained from the Barrick Meikle mine in Nevada. The bulk composition of those samples was $(Ba_{0.91}, Sr_{0.09})SO_4$, as analyzed by XRAL Laboratories, Canada. The presence of strontium (Sr) in barite crystals is common. The crystal was freshly cleaved by a sharp blow with a knife blade placed on a (210) face. Observations of these freshly cleaved (001) surfaces were made with NC-AFM prior to any treatments. Subsequent observations of barite dissolution were made on (001) surfaces that had been etched at room temperature in unstirred solutions in a 10 ml glass reactor. The etchants used were deionized water and DTPA solutions. The samples were washed with 0.1 M HCl (~ 10 s) and deionized water, and then dried in an oven before mounting on a steel disk. A brief rinse with HCl was necessary to avoid the deposition of DTPA and/or DTPA-Ba clusters during drying. NC-AFM investigations of the dissolution of barite in 0.1 M HCl showed that the etching effect after 10 s was very small and could be neglected compared to the effect of the DTPA solution.

2.2. DTPA solution at pH > 12

DTPA obtained from GFS Chemicals Co., was added to 90 ml 1.5 M NaOH solution. The pH was monitored during the addition of 7.08 g DTPA such that a pH > 12 was maintained. Final dilution to 100 ml with deionized water and mixing were then performed to prepare 0.18 M DTPA solutions.

2.3. Apparatus

A Park Scientific Instruments (PSI) Autoprobe CP Scanning Probe Microscope (SPM) was operated in non-contact mode. All experiments were performed in air and at room temperature using commercially available triangularly shaped Si cantilevers manufactured by PSI. These have a resonance frequency of about 280 kHz and a spring constant of about 13 N/m.

3. Results and discussion

3.1. (001) Surface structure of barite

$BaSO_4$ (barite) has an orthorhombic structure (space group P_{nma}) with lattice constants: $a = 8.8842$ Å, $b = 5.4559$ Å, $c = 7.1569$ Å, and $Z = 4$. The distance from a barium cation to one of the twelve nearest-neighbor oxygens ranges from 2.765 to 3.315 Å [24]. In a bulk barite crystal, each atom is surrounded in its rhombohedral network to optimize the binding energy. Each barium cation is coordinated to eight oxygen atoms of six SO_4^{2-} (sulfate) anions. Each oxygen atom of the sulfate anions is coordinated to two barium cations. Relaxation and reconstruction of the (001) surface are thought to be slight [25], and we assume that the computer models of the ideally terminated structure shown in Fig. 1(A) and 1(B) fairly represent the barite (001) surface. The (001) surface of barite is one of the two most common surfaces by far that are observed in geological crystals and experimental studies [26]. It is also found to be one of the two lowest energy surfaces in modeling studies [25,27].

3.2. Morphology of the cleaved (001) surface

NC-AFM images of a freshly cleaved barite (001) surface are shown in Fig. 2. These images are in agreement with reports by Putnis et al. [11] that barite has a high density of cleavage steps. The flat area in Fig. 2(A) contains several relatively smooth cleavage steps. However, Fig. 2(B) shows many sharp 'V-shape' or 'lightning pattern' steps. The topography of a freshly cleaved (001) surface is very different when observed over large areas on a micrometer scale [11,28]. Generally speaking, these steplines indicate the direction and velocity of crack propagation [29]. Based on the unit cell dimension along the c axis (i.e. $c = 7.16$ Å), the height of the steps in Fig. 2(A) is about one unit cell. In Fig. 2(B) the steps have a height of one or multiples of one unit cell. On some samples, the terraces shown in Fig. 2(A) were covered with granular particles. These might have been due to an immediate reaction between the barite surface and moisture in the surrounding

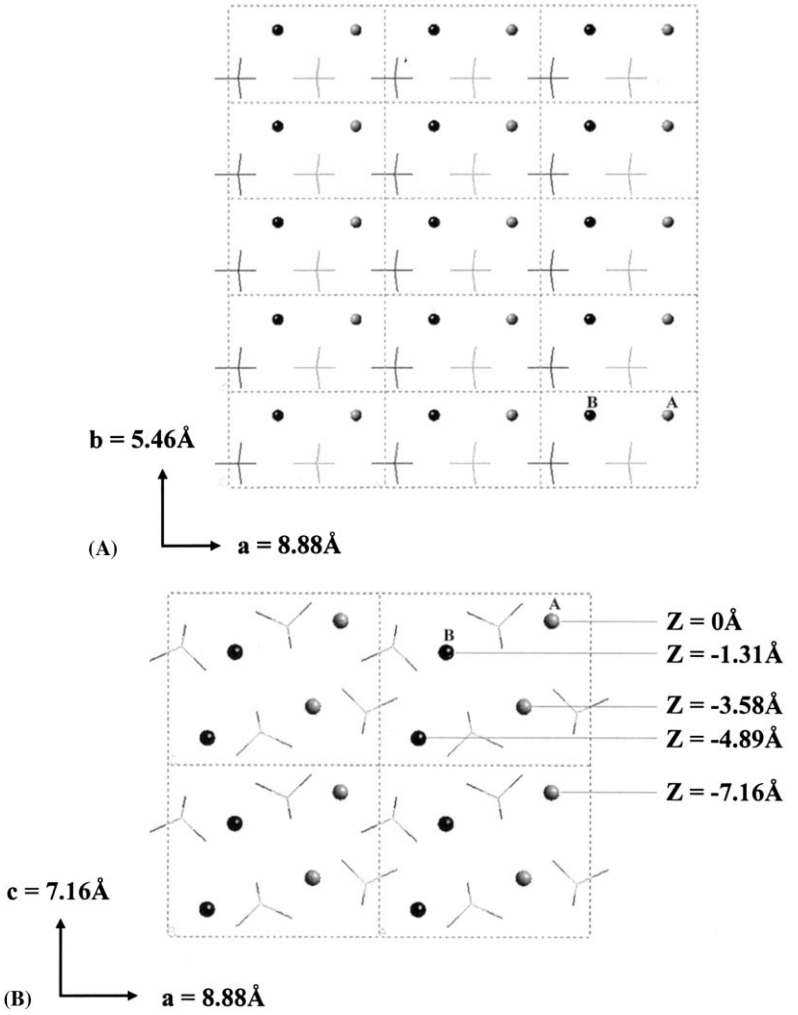

Fig. 1. Computer models of the $BaSO_4$ (001) surface. (A) Top view: the topmost half of one unit cell (c/2) is pictured schematically looking down at the surface along the c axis direction. The topmost Ba^{2+} cations at $z = 0$ (marked as A) are represented by lighter gray balls. The Ba^{2+} cations at $z = -1.31$ Å (marked as B) are represented by darker balls. The lighter tetrahedral 'sticks' represent SO_4^{2-} anions that are below the topmost Ba^{2+} cations. The darker tetrahedral 'sticks' represent SO_4^{2-} ions that are above the lower Ba^{2+} cations. The rectangular unit cell is shown by dashed lines. (B) Side view: the structure of the (001) surface is shown along the b axis direction. The first row of Ba^{2+} cations are defined at height $z = 0$, and then other deeper Ba^{2+} cations occur at $z = -1.31$ Å, -3.58 Å, -4.89 Å, and -7.16 Å. The Ba^{2+} cations are represented as gray and black balls. There are two orientations of SO_4^{2-} anions, which are represented as tetrahedral stick figures (sulfur-gray; oxygen-black).

atmosphere and/or due to contaminants deposited on the barite surface.

3.3. Morphological changes of barite (001) etched in deionized water

A dissolution sequence for barite etching in deionized water is shown in Fig. 3. NC-AFM was used in an ex-situ mode to observe the dissolution of a barite (001) surface for up to one hour at room temperature. In the image of Fig. 3(A), taken after 5 min, only one triangular etch pit (marked as 1) was observed. It occurred on the (001) terrace and had a depth of one-half unit cell. The height of the steps in Fig. 3(A) is about one unit cell. There was no obvious etching feature

found at the edge of steps. After 60 min, both terraces (marked as 1) and steps exhibited dissolution features, as shown in Fig. 3(B) and Fig. 3(C).

Fig. 3(B) was observed in a region that was similar to the region in Fig. 2(A) with several 'smooth' steps prior to etching by water. After dissolution of the barite crystal in deionized water for 60 min, the 'smooth' steps were etched along the edge of steps, and the etch pits found on terraces with a triangular shape were of either one-half or one unit cell in height. Only a few etch pits were observed on terraces. Two opposite orientations of the triangular etch pits are shown in Fig. 3(B). The obtuse angles of the etch pits are approximately 101°. This suggests that the pits are bounded along [120] and [1$\bar{2}$0] directions, which is consistent with the results by Higgins et al. [30]. Because the {001} faces and the {210} side faces are the two lowest energy surfaces in barite crystals, the geometry of the etch pits is a result of minimizing the surface energy as shown by the scheme in Fig. 3 (D).

Fig. 3(C) was observed in a region that was similar to the region in Fig. 2(B) with several 'V-shape' steps prior to etching by water. After immersing the crystal in deionized water for 60 min, 'zigzag shaped' etch pits were found at the edges of steps with a height of one-half unit cell, and triangular etch pits with a height one unit cell were also found on the terraces. In comparison to the (001) surface in Fig. 3(B), more dissolution features were observed in Fig. 3(C). The crystal dissolution occurs preferentially at steps. This is expected because steps are generally more chemically reactive than terraces due to the lower coordination numbers present there. For Ba^{2+} cations at the top edge of a step, the number of nearest-neighbor SO_4^{2-} anions is reduced. Thus, Ba^{2+} cations at the steps have a lower coordination number and are more easily solvated by water molecules. Once the Ba^{2+} cations are dislodged, they are surrounded by 'cages' of water molecules. Concurrently, the SO_4^{2-} anions no longer have Ba^{2+} cations as nearest neighbors. Water molecules also readily solvate SO_4^{2-} anions, i.e. SO_4^{2-} anions are removed from the edges and surrounded by 'cages' of water molecules permitting the crystal to dissolve.

3.4. Morphological changes of barite (001) in DTPA solution

3.4.1. NC-AFM observations

In Fig. 4 we present a series of NC-AFM images for dissolution times up to 60 min at room temperature in 0.18 M DTPA aqueous solutions. The images shown here represent the general dissolution features on the flat (001) surface, because a comparison of different surface areas revealed a homogeneous dissolution of the (001) surface for a particular dissolution time.

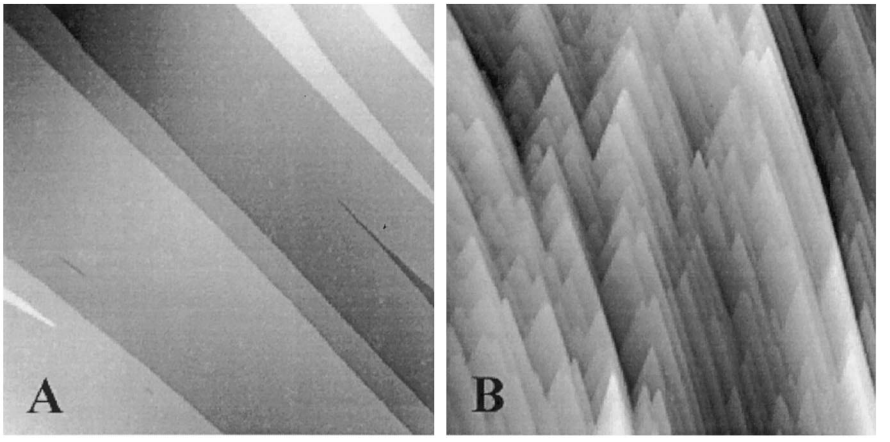

Fig. 2. Ex-situ NC-AFM images of a freshly cleaved barite (001) surface taken in air. Image size: 5 μm × 5 μm. Depth scale from black to white: (A) 4 nm, (B) 10 nm

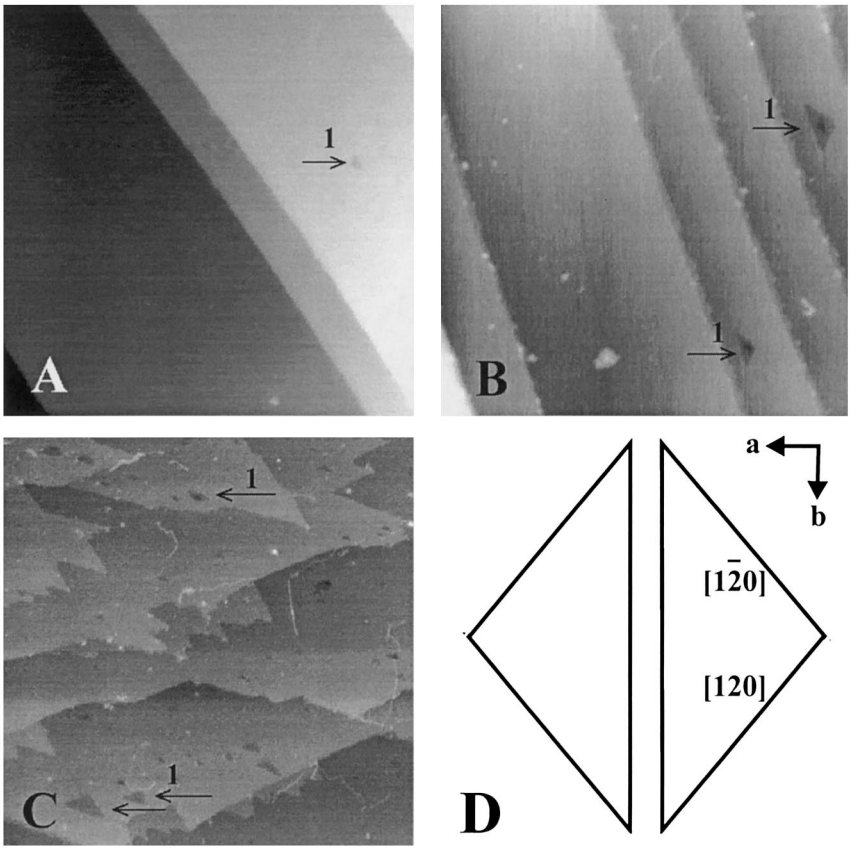

Fig. 3. Ex-situ NC-AFM images of the dissolution behavior of a freshly cleaved barite in water after (A) 5 min, and (B and C) 60 min. Image size: 1 μm × 1 μm. Depth scale from black to white: (A), (B) and (C) 3 nm. Fig. 3D shows a schematic drawing of the crystallographic orientation of etch pits on a barite (001) surface induced by water.

The etch pits produced by DTPA molecules dominated the dissolution of the flat (001) surface. In the first 15 min, as shown in Fig. 4(A), (B) and (C), features were observed on the terraces denoted as triangular etch pits (less than one unit cell in height) marked as '1', trapezoidal etch pits (less than one unit cell in height) marked as '2', and 'rice-shape' etch pits (one to four unit cells in height) marked as '3'. Also, ragged or zigzag steps with a height of less than one unit cell were common. In the beginning, these shallow features from barite dissolution were easily observed on the (001) surface. However, deeper and elongated etch pits with a 'rice shape' (dark areas of more than one unit cell in height) induced by DTPA molecules increased in size for increasing time as shown in Fig. 4(D)–(F) and overwhelmed the images.

$DTPA^{5-}$ molecules apparently removed the Ba^{2+} cations on the terraces in a fashion that created new steps parallel to each other as seen in Fig. 4(D)–(F). This also suggests that most of the step edges were composed of sulfate anions, which cannot complex with $DTPA^{5-}$. Most of these etch pits had flat bottoms as shown in Fig. 5. This suggests that DTPA dissolved the (001) surface in a layer-by-layer process. To reiterate, several different regions on the barite crystal were explored by NC-AFM and the results presented here were general.

The shallow etch pits developed a trapezoidal and/or trapezohedral shape (Scheme 2) as the dissolution time increased. Most of the angles at the ends of the larger etch pits were 58° for the

trapezoidal pits and 97° for the trapezohedral pits. This is shown more clearly in Fig. 5. The pits also grew deeper and longer (much more than one unit cell in depth and length) with increasing time. The deepest etch pit shown in each image of Fig. 4(A)–(F) was 20, 26, 30, 62, 130 and 310 Å,

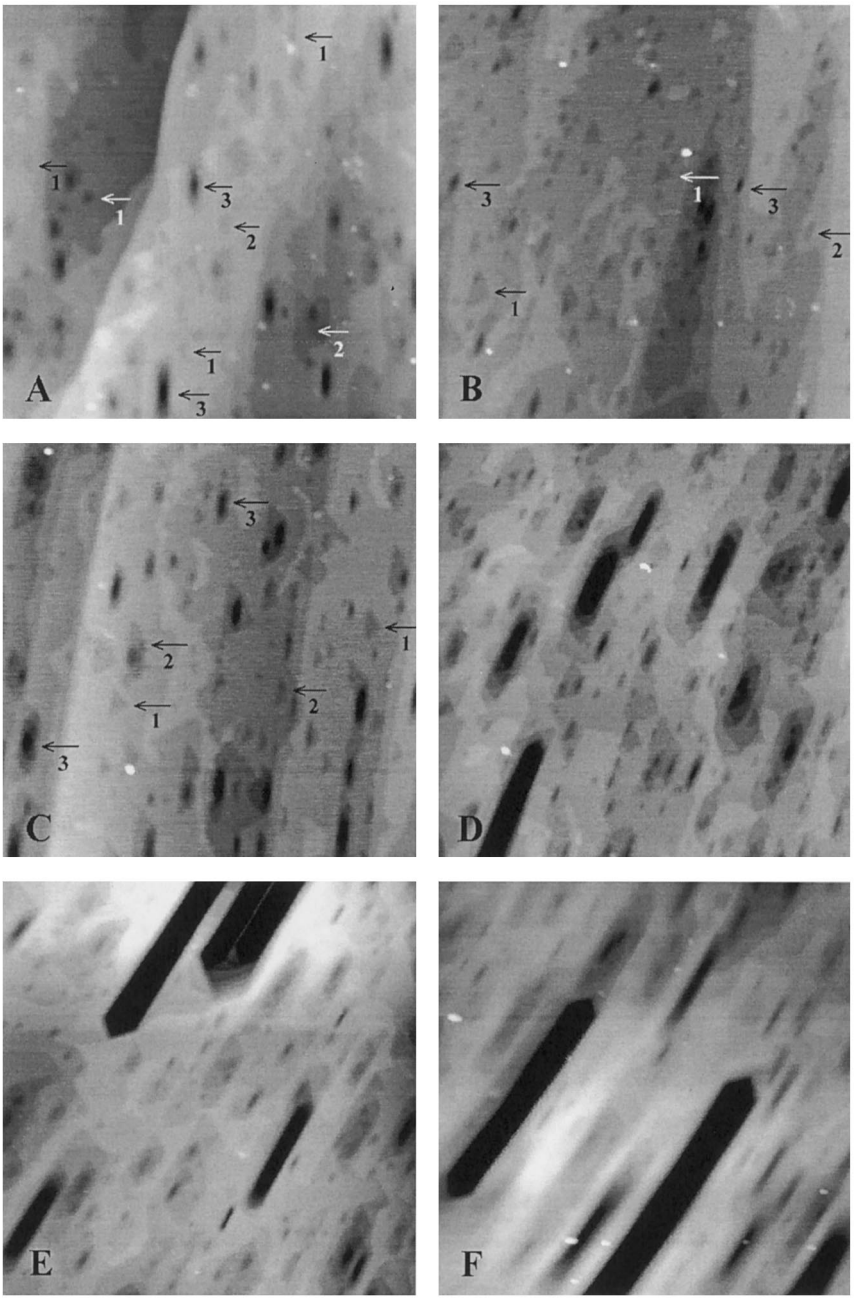

Fig. 4. Ex-situ NC-AFM images of the dissolution of a freshly cleaved barite in 0.18 M DTPA after (A) 5 min, (B) 10 min, (C) 15 min, (D) 25 min, (E) 40 min and (F) 60 min. Image size: 2 μm × 2 μm. Depth scale from black to white: (A), (B) and (C) 5 nm, (D) 8 nm, (E) 16 nm and (F) 40 nm.

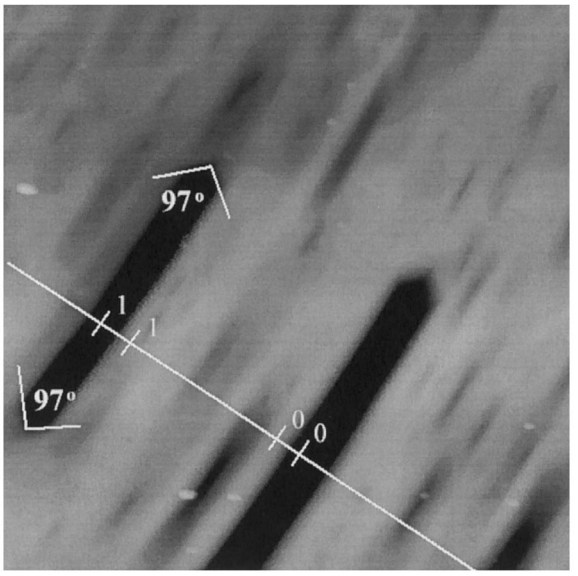

Fig. 5. A line profile measurement of Fig. 4(F) is shown. Flat bottom of the etch pits were often observed as shown for the '0, 0' pit here. The depths of the etch pits '1, 1' and '0, 0' are 306 Å, and 152 Å, respectively. The bottom of very deep etch pits cannot be measured accurately because of tip convolution effects.

respectively.

The orientation of the etch pits was along the crystallographic *b* axis, which is in agreement with the previous results by Putnis et al. [11]. Other directions for the etch pits, i.e. not along the *b* axis, were never observed. Also, the growth rate of etch pits along the *b* axis was much faster than along the *a* axis. These observations appear to be related to the spatial arrangement of the Ba^{2+} cations and the DTPA conformations possible on the (001) surface, but a detailed picture of these processes is still not completely developed.

By comparison to the etch pits induced by water, as shown in Fig. 3, the images of Fig. 4 show that the dissolution mechanism in DTPA aqueous solutions is different from that in water. Water is a small molecule relative to DTPA, so H_2O molecules can approach the (001) surface and interact with Ba^{2+} cations (or SO_4^{2-} anions) without strong steric hindrance. Therefore, in water (in the absence of DTPA) shallow (less than one unit cell height) etch pits developed, which were distributed randomly and mostly bounded by the lowest energy planes along the [120] and [1$\bar{2}$0] directions to form triangular features. Our model of the more complicated DTPA etching process is explained in more detail in Section 3.4.2

3.4.2. Proposed interfacial reaction mechanisms for barite etching by DTPA

Although $DTPA^{5-}$ forms a strong chelate in aqueous solution with free Ba^{2+} cations in a 1:1 ratio, it is unlikely that $DTPA^{5-}$ coordinates around only one Ba^{2+} cation on the flat barite terraces. This is because of steric hindrance by the barite surface when the oxygen donor groups approaching the cation. The trapezoidal shape of the etch pits suggests that one $DTPA^{5-}$ may bind two Ba^{2+} cations in the topmost layer by orienting the molecule at an angle of 58° with respect to the *b* axis. Removal of two such cations could result in an etch pit bounded along the [110] and [010] directions, as first suggested by Putnis et al. [11]. This was also simulated by Blanco et al. [27]. A model of a $DTPA^{5-}$ conformation that would bind in this fashion is shown in Fig. 6(A). The distances between the two coordinating negatively charged oxygens in $DTPA^{5-}$ and the Ba^{2+} cations are 2.7 Å and 2.5 Å, respectively.

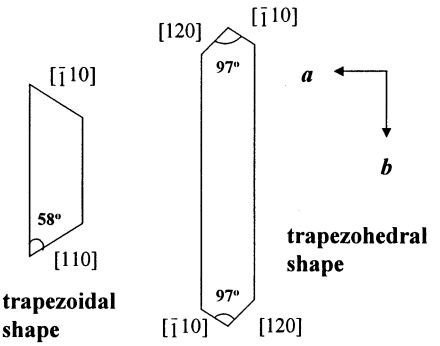

Scheme 2.

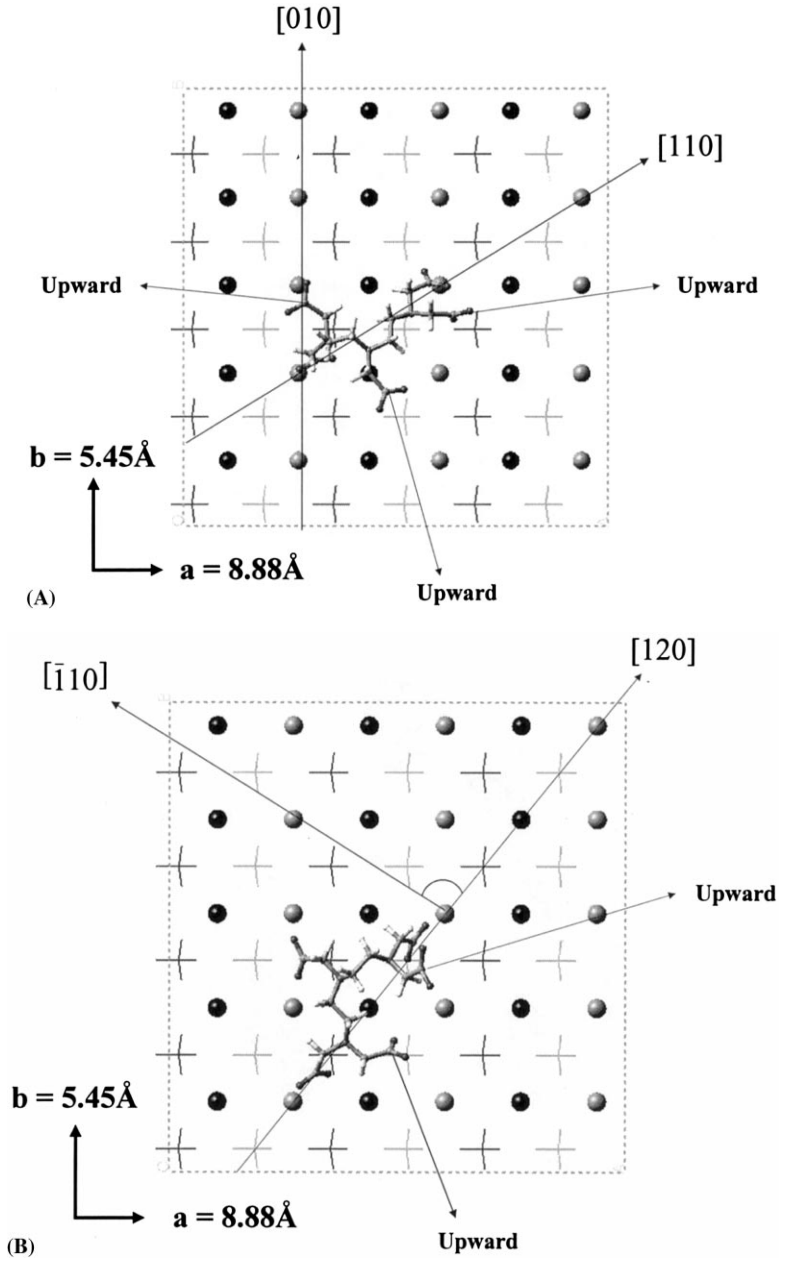

Fig. 6. Two possible conformations of $DTPA^{5-}$ on the barite (001) surface. (A) $DTPA^{5-}$ binds two topmost Ba^{2+} cations using negatively charged oxygens in two acetate groups with the other three acetate groups oriented upward, away from the surface. (B) $DTPA^{5-}$ binds three topmost Ba^{2+} cations using negatively charged oxygens in three acetate groups with the other two acetate groups oriented upward, away from the surface.

In contrast to Putnis et al. [11], our observation of the trapezohedral shape etch pits with an angle of 97° suggests that $DTPA^{5-}$, which can fully extend to 11 Å, may orient itself to also allow three acetate groups to coordinate simultaneously to three Ba^{2+} cations on the topmost layer. The

distances between the three coordinating negatively charged oxygens in $DTPA^{5-}$ and the Ba^{2+} cations are 4.05Å, 4.30Å and 4.20Å. The trapezohedral shape of the etch pits may be triggered by $DTPA^{5-}$ binding to three Ba^{2+} cations in addition to concurrent binding of a $DTPA^{5-}$ molecule to two Ba^{2+} cations on the topmost surface layer. Removal of five such cations via coordination by two DTPA molecules in this manner on the (001) surface leads directly to a 97° angle at the end of an etch pit. Pits such as these are bounded along the [$\bar{1}$10] and [120] directions. This can be simulated as shown in Fig. 6(B) using the commercial *Cerius2* simulation package. The conformation of the fully deprotonated $DTPA^{5-}$ was used to illustrate the relationship between the atomic structure of the barite (001) surface and the $DTPA^{5-}$ conformation for the proposed model above.

However, much work still needs to be done to further elucidate mechanistic details. For example, there probably exist other DTPA conformations on the (001) surface and further work to measure the interactions between the solvent, chelating agents, and mineral surface is required to insure that morphological, stereochemical, and electrostatic requirements are satisfied.

4. Conclusions

Ex-situ observations of etch pits by NC-AFM provide a powerful view of the sample microtopography for dissolution features in the barite (001) surface. These morphological features provide useful information about the nature of the dissolution phenomena. NC-AFM images of dissolution etch pits caused by either deionized water or 0.18 M DTPA aqueous solutions at $pH > 12$ are quite different. Dissolution in pure water proceeds via attack of sites such as steps, kinks and other defects on the (001) surface. This leads to shallow zigzag-shaped etch pits on the step edges. In DTPA solutions, deep etch pits on the (001) terraces are created perpendicular to the (001) surface and longer along the *b* axis. In order to explain the observed etch pit geometries, we propose a new model for the interaction between $DTPA^{5-}$ and the barite (001) surface wherein $DTPA^{5-}$ adopts a conformation to bind three Ba^{2+} cations on the (001) topmost layer. Molecular modeling shows that the $DTPA^{5-}$ ligand can indeed bind two and three Ba^{2+} cations on the barite (001) surface.

Acknowledgements

Financial support from the Z.A. Kaprielian Technology Innovation Fund to B.E. Koel and from the Chevron Petroleum Technology Company (CPTC) to T.F. Yen are gratefully acknowledged. We thank the Laboratory for Molecular Robotics at USC for use of the AFM facility. The authors also thank Dr Alden Carpenter for his assistance with barite cleavage, Dr H. Chen and Dr E. Daniels for discussions at CPTC, and Dr M. Blanco, Dr Y.H. Jang and Professor W.A. Goddard III in the Materials and Process Simulation Center at CIT for their help with the computer models.

References

[1] O.J. Vetter, J. of Petroleum Technol., December (1976) 1403.
[2] T. Haarberg, I. Selm, D.B. Granbakken, T. Fstvold, P. Read, T. Schmldt, SPE Production Engineering, Feburary (1992) 75.
[3] E. Hogfeldt, Stability Constants of Metal-ion Complexes. Part A: Inorganic Ligands, IUPAC Chemical Data Series No. 21, Pergamon Press, Oxford, 1982.
[4] A.L. Smith, J. Petroleum Technol., June (1987) 697.
[5] R.L. Morris, J.M. Paul, United States Patent 4 980 077, December 1990.
[6] A. Putnis, C.V. Putnis, J.M. Paul, SPE 29094, presented at the SPE International Symposium on Oilfield Chemistry, San Antonio, TX, Feburary (1995) 773.
[7] F. Basolo, R.C. Johnson, Coordination Chemistry: The Chemistry of Metal Complexes, W.A. Benjamin, 1964.
[8] R.M. Smith, A.E. Martell, R.J. Motekaitis, Critical Stability Constants Database, 46, NIST, Gaithersburg, MD, USA, 1993.
[9] P.E. Hillner, A.J. Gratz, S. Manne, P.K. Hansma, Geology 20 (1992) 359.
[10] A.J. Gratz, P.E. Hillner, P.K. Hansma, Geochim. Cosmochim. Acta 57 (1993) 491.
[11] A. Putnis, J.L. Junya-Rosso, M.F. Hochella Jr, Geochim. Cosmochim. Acta 59 (1995) 4623.

[12] D. Bosbach, M.F. Hochella, Chem. Geol. 132 (1996) 227.
[13] C. Hall, D.C. Cullen, AIChE J. 42 (1996) 232.
[14] C.M. Pina, D. Bosbach, M. Prieto, A. Putnis, J. Crystal Growth 187 (1998) 119.
[15] P.M. Dove, M.F. Hochella, Geochim. Cosmochim. Acta 57 (1993) 705.
[16] D. Bosbach, W. Rammensee, Geochim. Cosmochim. Acta 58 (1994) 843.
[17] D.W. Britt, V. Hlady, Langmuir 13 (1997) 1873.
[18] A. Seo, H. Shindo, Appl. Surf. Sci. 82/83 (1994) 475.
[19] G. Binnig, C.F. Quate, C. Gerber, Phys. Rev. Lett. 56 (1986) 930.
[20] Y. Martin, C.C. Williams, H.K. Wickramasinghe, J. Appl. Phys. 61 (1987) 4723.
[21] R. Lüthi, E. Meyer, L. Howald, H. Haefke, D. Anselmetti, M. Rüetschi, T. Bonner, R.M. Overney, J. Frommer, H.-J. Güntherodt, J. Vac. Sci., Technol. B 12 (1994) 1673.
[22] R.M. Overney, H. Takano, M. Fujihira, E. Meyer, H.-J. Güntherodt, Thin Solid Films 240 (1994) 105.
[23] R. Resch, G. Friedbacher, M. Grasserbauer, Fres. J. Anal. Chem. 358 (1997) 352.
[24] R.J. Hill, Can. Mineral. 15 (1977) 522.
[25] N.L. Allan, A.L. Rohl, D.H. Gay, R.A. Catlow, R.J. Davey, W.C. Mackrodt, Faraday Discuss. 95 (1993) 273.
[26] S.N. Black, L.A. Bromley, D. Cottler, R.J. Davey, B. Dobbs, J.E. Rout, J. Chem. Soc. Faraday Trans. 87 (1991) 3409.
[27] M. Blanco, Y. Tang, P. Shuler, W.A. Goddard III, Mol. Eng. 7 (1997) 491.
[28] M.F. Hochella Jr., Reviews in Mineralogy, vol. 23, 1990, Ch. 3.
[29] L.S. Wainer De, G.A. Bassett, Phil. Mag. A 38 (1978) 707.
[30] S.R. Higgins, G. Jordan, C.M. Eggleston, K.G. Knauss, Langmuir 14 (1998) 4967.